Intermetallics 150 (2022) 107685

Contents lists available at ScienceDirect

Intermetallics

journal homepage: www.elsevier.com/locate/intermet

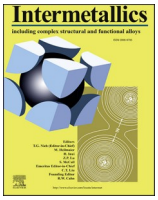

Unraveling hot deformation behavior and microstructure evolution of nanolamellar TiAl/Ti3Al composites

Yang Chen [a], Jia Li [a,*], Bin Liu [b,**], Jian Wang [c], Nan Liu [c], Siwei Ren [a], Peter K. Liaw [d], Qihong Fang [a]

[a] State Key Laboratory of Advanced Design and Manufacturing for Vehicle Body, College of Mechanical and Vehicle Engineering, Hunan University, Changsha, 410082, PR China
[b] State Key Laboratory of Powder Metallurgy, Central South University, Changsha, 410083, PR China
[c] State Key Laboratory of Porous Metal Materials, Northwest Institute for Nonferrous Metal Research, Xi'an, 710016, China
[d] Department of Materials Science and Engineering, The University of Tennessee, Knoxville, TN, 37996, USA

ARTICLE INFO

Keywords:
Nanolamellar TiAl/Ti_3Al composite
Temperature
Deformation gradient
Microrotation
Deformation twinning
Phase transformation

ABSTRACT

An in-depth understanding of the deformation behavior of a nanolamellar TiAl/Ti_3Al composite is prerequisite to control the mechanical properties of this material. Nevertheless, to obtain the excellent performance, the role of microstructure evolution on the deformation mechanism maps at a wide temperature range is still required. To this end, the effect of temperature on the compressive response and deformation mechanism of a nanolamellar TiAl/Ti_3Al composite is investigated using molecular dynamics simulations. The deformation-induced $\alpha_2 \rightarrow \gamma$ phase transformation results in the softening, and the deformation twinning causes the strain hardening. The high temperature reduces the local shear strain along the interface, to enhance the deformation capacity of the γ phase. At a low strain, the dislocation slip on the single slip system is the dominant deformation mode; at a medium strain, the phase transformation controls the plastic deformation; at a high strain, the deformation twinning associated with the activation of the multi-slip systems is responsible for the late plastic stage. The phase interface bents towards the γ phase, and then the α_2 phase grows up, resulting in the evolution of the dynamic complex microstructures. The origin of the nanoscale plasticity event depends upon the atomic-scale deformation gradient field and the atomic-scale microrotation field. The current temperature-dependent deformation mechanism maps provide an insight into the design and fabrication of the advanced nanolamellar TiAl/Ti_3Al composites with outstanding strength and ductility.

1. Introduction

The TiAl alloys have various application characteristics conducive to the high-temperature structural materials, including low density, high strength/hardness at high temperatures, and excellent oxidation/creep resistance at elevated temperatures [1]. Thus, the TiAl alloys are expected to replace the current Ni-based superalloy, and become a new generation of the lightweight high-temperature structural materials, which have a good application in the aviation field [2,3]. However, the poor room-temperature plasticity, low fracture toughness, and high crack-growth rate in the TiAl alloys restrict their applications in key parts [4,5], such as aero-engine. This urgent problem that the plasticity of the TiAl alloy is increased while its strength decreases slightly, should be solved.

Through the reasonable adjustment and optimization of the microstructures, the lack of the tensile plasticity and fracture toughness of the TiAl alloy can be compensated to a certain extent [6]. The lamellar microstructure has a great effect on improving the mechanical properties of the TiAl alloys, and this issue has been in focus of extensive research [7]. The effect of the lamellar orientation on the strength in the Ti45Al2Nb2Mn alloy is investigated by the micropillar compression, and the strength at 90° loading is larger than that at 45° loading [8]. The lamellar morphology of an γ phase appears in the Ti48.6Al4.1Nb0.7W0.4Si0.5C0.1B and Ti47.4Al5.6Nb0.4W alloys prepared by spark plasma sintering and a heat treatment, and then increases their strength and creep resistance [9]. Owing to the effects of size and

* Corresponding author.
** Corresponding author.
E-mail addresses: lijia123@hnu.edu.cn (J. Li), binliu@csu.edu.cn (B. Liu).

https://doi.org/10.1016/j.intermet.2022.107685
Received 28 March 2022; Received in revised form 27 July 2022; Accepted 4 August 2022
Available online 26 August 2022

interface, the multilayer materials significantly enhance the ductility and fracture toughness, and they have been developed as a new class of the microstructural materials [10].

Due to that the working conditions are complex, the plastic-deformation mechanism of the lamellar TiAl alloy needs to be studied under different loading conditions. The pre-deformation treatment of the TiAl alloy by the high-temperature torsion leads to the high strength and ductility owing to a gradient microstructure [11]. The superplasticity of the Ti42.5Al8Nb0.2W0.2B0.1Y alloy at 1000 °C (a tensile elongation up to 380%) is caused by the main deformation mechanism of the grain-boundary slip accompanied by the discontinuous dynamic recrystallization [12]. However, in order to expand the application range of the TiAl alloy, a deep understanding of the effect of microstructure evolution on the deformation behavior for a wide temperature range is still required for obtaining better mechanical properties.

Owing to the constraints of the sample preparation and testing technology, it is difficult for the experimental methods to clarify the influence of the dynamic microstructural evolution on deformation mechanism of the TiAl alloy at a wide temperature range. However, the evolution of the multiphase structure during the hot deformation plays an important influence on the deformation behavior in the lamellar TiAl alloys [13,14]. A molecular dynamics (MD) methods can simulate the complex environmental conditions, and obtain the dynamic evolution of the microstructures at the corresponding plastic strain, to essentially reflect the internal relationship of the microstructures and mechanical properties [15,16]. The effects of temperature, stress, and grain size on the creep properties of the TiAl alloy are studied via MD simulations, revealing the creep mechanisms of dislocation slip and grain-boundary diffusion in the steady-state deformation stage [17]. The deformation mechanism of the lamellar TiAl alloys during the sliding of the γ/γ interface is revealed by MD simulations, including the interface migration, twin nucleation and migration, dislocation nucleation and grain-boundary sliding [18].

The objective of this study is to investigate the effect of phase interface on the mechanical properties and deformation mechanisms in the nanolamellar TiAl/Ti_3Al composites under the hot compressive deformation by MD simulations. The underlying cause for the redistribution of strains is analyzed to determine a way to enhance the ductility. First, the nanolamellar TiAl/Ti_3Al composite is constructed, and then suffers from the uniaxial compressive deformation at a wide temperature range. Subsequently, the microstructure and atomistic local strain for the three key stages are characterized. Our study reveals the occurrence of phase transformation and deformation twinning under the hot deformation to improve the strength and ductility [19]. The organization of the current work is as follows: Section 2 outlines the model and method. In Section 3, the mechanical response and microstructural evolution of the nanolamellar TiAl/Ti_3Al alloys are presented, and the results are analyzed and discussed. Finally, some conclusions are summarized in Section 4.

2. Model and method

The TiAl model is composed of γ-TiAl and α_2-Ti_3Al. γ-TiAl has a tetragonal primitive crystal lattice with an $L1_0$ structure (Pearson symbol tP4, space group P4/mmm), and α_2-Ti_3Al has a hexagonal-close-packed (HCP) structure. Here, a size of the TiAl sample is 270 Å (x) × 150 Å (y) × 598 Å (z), and the total number of atoms is 1,535,328. A periodic boundary condition is used in the z direction, and the free surfaces are employed in x and y directions. In the γ-TiAl phase, the crystalline orientation is x-$[\bar{1}\bar{1}2]$, y-$[1\bar{1}0]$, and z-[111]; In the α_2-Ti_3Al phase, the crystalline orientation is x-[1100], y-$[11\bar{2}0]$, and z-[0001]. All simulations are performed using open source atomic/molecular large-scale parallel simulator (LAMMPS) code [20]. The time step is 1 fs. Before the loading, the Nose-Hoover method is used to relax the model at 300 K and 0 bar for 60 ps under a constant-pressure and constant-temperature (NPT) ensemble [21,22]. Hence, the total energy of the system reaches a stable state. Subsequently, the system is loaded with a constant temperature, and with the strain rate of 1×10^8 s^{-1} in the z direction. The visual tool of OVITO [23] is used to obtain the configuration of the atomic structure, and the crystal defects are analyzed by the common neighbor analysis (CNA) [24] (Fig. 1). The green atoms represent the $L1_0$ phase, the blue atoms represent a body-centered-cube (BCC) phase, the red atoms represent an HCP phase, and the white atoms represent unknown local structures. From Fig. 1b, the interfacial phase interface occurs in the nanolamellar TiAl/Ti_3Al composite.

The embedded-atom-method (EAM) potential is chosen for the calculation of TiAl intermetallic compounds [25], which can be expressed by

$$E = F_\alpha \sum_{j \neq i} \rho_i(R_{i,j}) + \frac{1}{2} \sum_{j \neq i} \varphi_{\alpha,\beta}(R_{i,j}) \tag{1}$$

where E is the total energy of the atomistic system comprising the sum of the embedding energy, F, on atom, i, and the short-range pair potential energy, φ, ρ is the electron density, and α and β are the element types of atoms, i and j. The pair potential term, φ, is the electrostatic contribution. Here, the EAM potential for TiAl alloys developed by Zope and Mishin can be a good agreement with the experiment [25].

To visualize the plastic shearing of the TiAl alloys during the deformation, the local shear strain of each atom, i, in the system is calculated, using the equation [26,27]:

$$\eta_i^{Mises} = \sqrt{\frac{1}{6}\left[(\eta_x - \eta_y)^2 + (\eta_y - \eta_z)^2 + (\eta_z - \eta_x)^2 + \eta_{xy}^2 + \eta_{yz}^2 + \eta_{zx}^2\right]} \tag{2}$$

where η_x, η_y, η_z, η_{xy}, η_{yz} and η_{zx} are the components of the Lagrangian strain matrix for a specific atom. Here, the atomistic strain analysis is performed, employing the OVITO, which has been applied in the previous atomic simulations [28–30]. The atomic-level strain tensors can be estimated based on the displacement gradient tensor of each atom

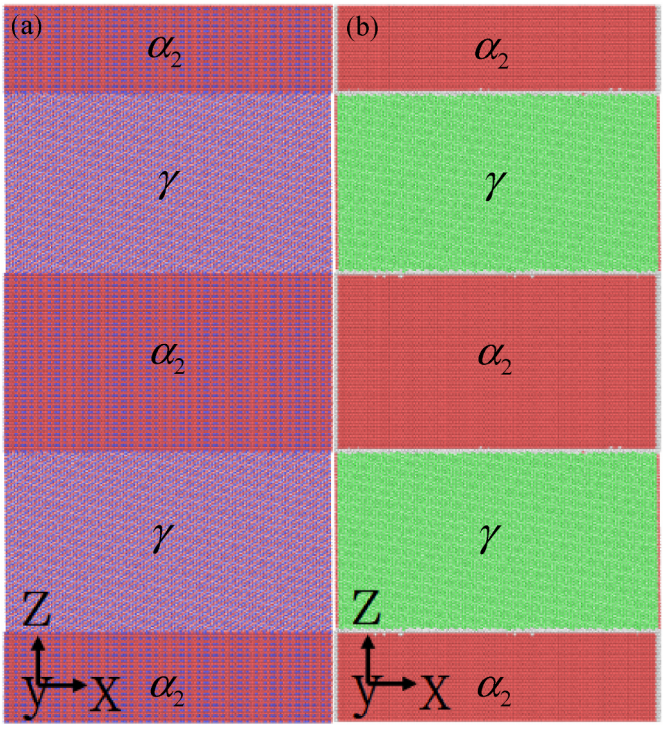

Fig. 1. The TiAl model, where atoms are colored based the atom type (a) and CNA (b). In (a), Ti, and Al. In (b), $L1_0$ structure, HCP structure, BCC structure, and other structure.

corresponding to the distance from the initial-and-undeformed configuration at the given temperature to the deformed configuration at the given temperature. Thus, the corresponding strain can be obtained at the temperatures of 300 K, 1100 K, 1300 K, and 1500 K.

3. Results and discussion

The compressive curves of the TiAl sample at different temperatures are plotted in Fig. 2. Based on the stress evolution, the four stages are divided, and include the elastic stage, yielding stage, softening stage, and hardening stage. Fig. 2a suggests that the stress decreases sharply after the yielding stage, and then increases with the increasing strain. This observation has been reported in the nanocrystalline TiAl alloy [31] and dual-phase TiAl alloy [32], where the TiAl alloy softens with the continuous loading. The potential physical mechanisms for such a behavior have been discussed by the previous work [33]. For example, no dislocations at the initial stage of deformation are contained in the material which firstly have to be generated causing a steep rise of the stress for the MD simulations with the high strain rate applied [33]. As the loading temperature increases, the elastic modulus decreases from 160 GPa at 300 K to 107 GPa at 1500 K (Fig. 2b). The yielding strength is 3.16 GPa at 300 K, 2.64 GPa at 1100 K, 2.46 GPa at 1300 K, and 2.05 GPa at 1500 K (Fig. 2b), showing the temperature-dependent mechanical properties in the TiAl alloys. In addition, the flow stress is about 500 MPa at 300 K, which corresponds approximately to the experiment [34]. Recently, from the compression tests of a nanocrystalline TiAl, the yielding stress and Young's modulus decrease the increasing temperature, because most atoms vibrating near their equilibrium positions reduce the bond energy [31].

To study the effect of temperature on the yielding mechanism, the atomic configuration of lamellar TiAl alloys at a compressive strain of 3% is presented in Fig. 3a. As a result, the dislocations are nucleated from the interface, and slip towards the other side of the interface [28,29]. Then, this process keeps on repeating, to adapt to the increased strain. In the yielding stage, the single slip system is activated in the α_2 phase. For the γ phase, a few dislocations are generated, due to the higher critical stress for dislocation nucleation compared to that of the α_2 phase [29]. At high temperatures, the stacking faults basically run through the α_2 phase, to bear the main plastic deformation. Therefore, the dislocation glide is the dominant deformation mechanism at the low strain and in a wide temperature range. In order to understand the atomic arrangement under the compressive deformation, the local shear-strain evolution of the lamellar TiAl alloys at the fixed strain of 3% is presented in Fig. 3b. The isolated shear-transformation zones (STZs) are activated in the α_2 phase [27,29]. With the increased temperature, the STZs take place along the interface with the high shear stress (Fig. 3b). Thus, the α_2-γ interface would play a key role in the hot deformation process.

At the strain of 6%, Fig. 4a shows the microstructure of the TiAl sample. The phase transformation from HCP to $L1_0$ structure occurs in the γ-TiAl, leading to the softening phenomenon (Fig. 2a). The process of deformation-induced $\alpha_2 \rightarrow \gamma$ phase transformation has been reported in the early experiment [35], and the atomic-scale simulation results for $\alpha_2 \rightarrow \gamma$ phase transformation are described in Fig. 5. Apart from two super ledges along the α_2-γ interface, the geometric features of the phase interface are almost atomically flat and perfectly coherent [36]. This $\alpha_2 \rightarrow \gamma$ phase transformation has been frequently reported in the TiAl alloy during the deformation [35–38]. Fig. 6 shows the dynamic distribution of elements during the phase transformation. The increasing temperature would affect the microstructures in the α_2-Ti_3Al, where the density of stacking faults reduces during hot deformation. The local strain in Fig. 4b shows that the local high-strain regions disappear gradually in the γ phase with the increasing temperature. This important phenomenon would inhibit the crack initiation, and improves the deformation capacity of the γ phase.

Fig. 7a shows the dislocation slip and deformation twinning during the strain hardening stage. The multi-slip systems (see the black circle of Fig. 7a) are activated in the TiAl sample, which cause not only the high work hardening but also the good plastic deformation [39,40]. The increasing temperature leads to that the interface bends to the γ phase (Fig. 7a). This process would cause the dynamic complex microstructure evolution, revealing the growth of the α_2 phase. In addition, the deformation twinning occurs, and the continuous dynamic processes are captured in Fig. 8. This result has been observed in the deformed TiAl alloy [41,42]. The high-density stacking faults produce a large number of STZs in the sample (Fig. 7b). At the same time, a shear band is generated as a result of the activation, percolation, and annihilation of STZs [43].

The deformation gradient in the finite plasticity plays a key role in describing the discrete evolution of the stresses, which would affect the material-deformation behaviors [44]. Fig. 9 shows the component, zz, of the deformation gradient at an atomic scale [44,45]. It suggests a detailed information concerning the deformation path of atoms traversed by the bending interface. Although the atoms of the red and blue regions in every phase currently reside in the equilibrium positions, the deformation gradient provides some degree of the deformation history [45]. The higher temperature would result in a larger deformation-gradient region, due to that the local lattice instability of the nanolamellar TiAl/Ti_3Al composites occurs at elevated temperatures. The obvious deformation-gradient fields take place in the small regions near the interface boundary (Fig. 9). In addition, the complex deformation-gradient region, including the strong interface strain and interlaminar strain, occurs (Fig. 9). More importantly, the phase interface prevents the expansion of the deformation gradient, where the value of the deformation gradient has changed greatly (Fig. 9).

Fig. 10 shows the atomic-scale rotation around the y axis during the

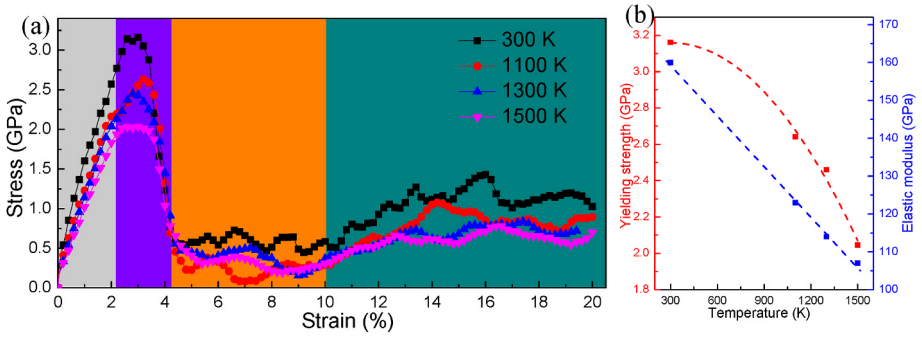

Fig. 2. The strain-stress relationship for different temperatures (a). The yielding stress and elastic modulus vs. the temperature (b).

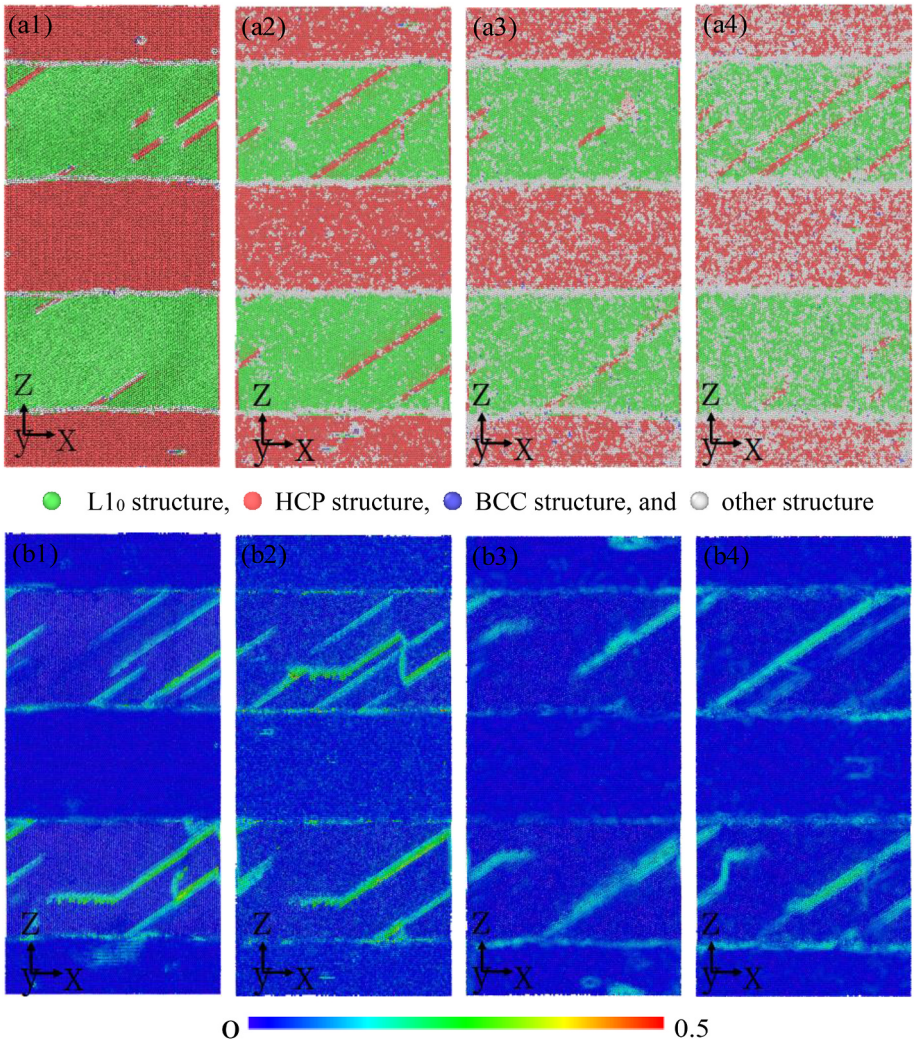

Fig. 3. The microstructure evolution, and the local shear-strain distribution for the temperatures of 300 K (a1, b1), 1100 K (a2, b2), 1300 K (a3, b3), and 1500 K (a4, b4) at the strain of 3%.

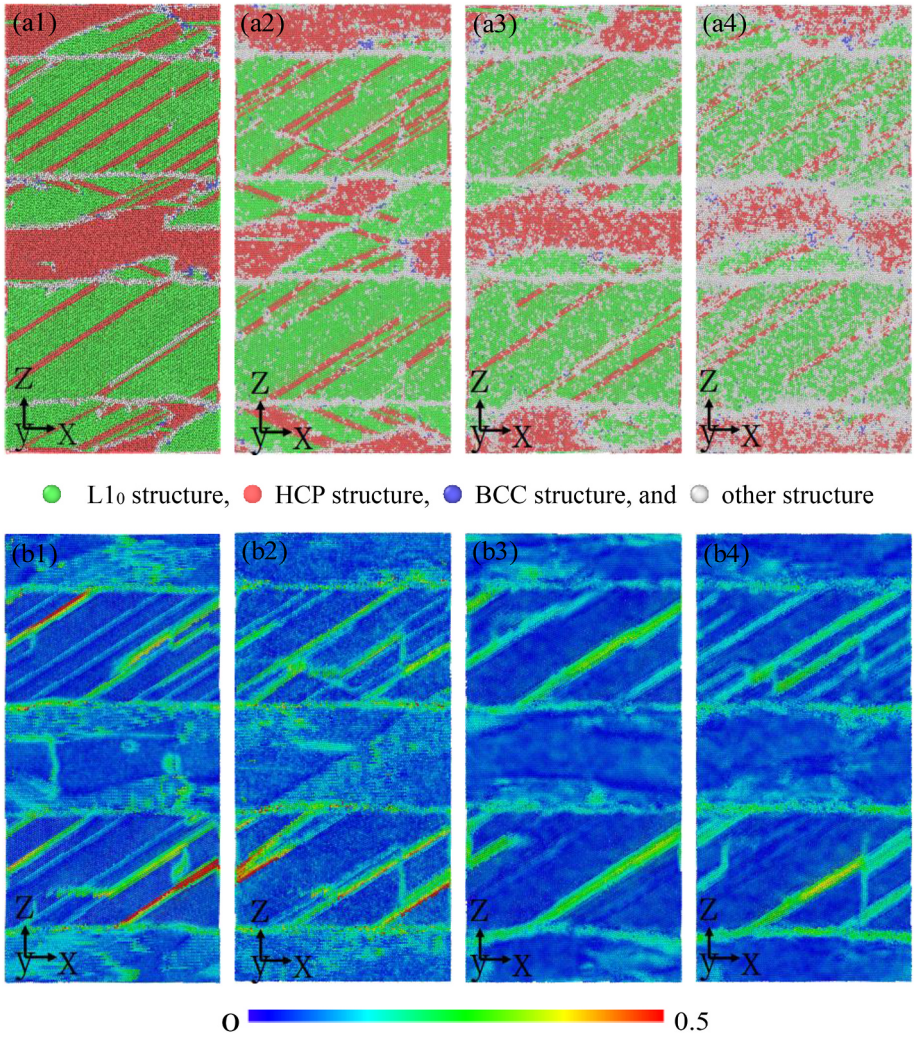

Fig. 4. The microstructure evolution, and the distribution of the corresponding strain for the temperatures of 300 K (a1, b1), 1100 K (a2, b2), 1300 K (a3, b3), and 1500 K (a4, b4) at the strain of 6%.

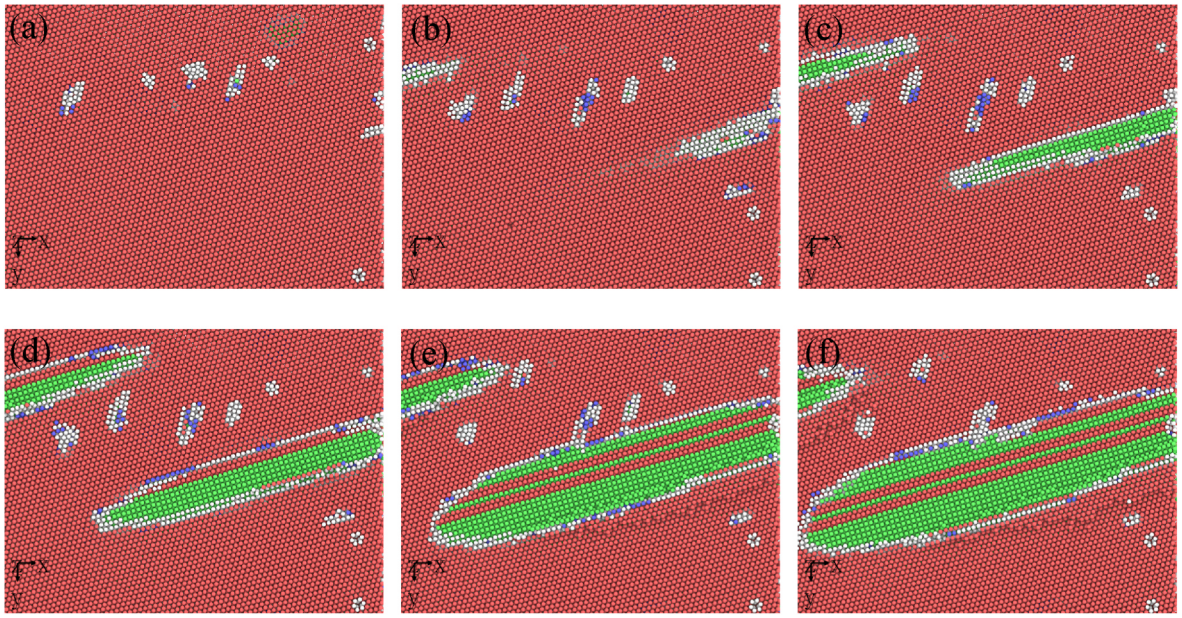

Fig. 5. The $\alpha_2 \rightarrow \gamma$ phase transformation with the increasing strain of 4% (a), 6.4% (b), 6.5% (c), 6.6% (d), 6.8% (e), and 6.9% (f). $L1_0$ structure, HCP structure, BCC structure, and other structure.

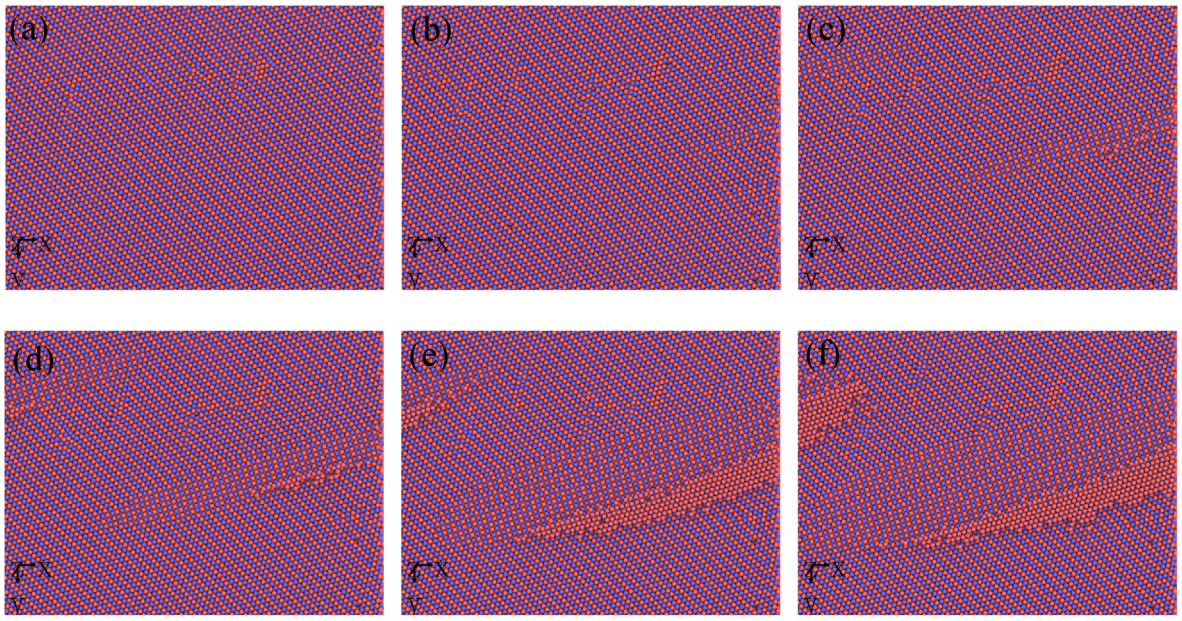

Fig. 6. The $\alpha_2 \rightarrow \gamma$ phase transformation with the increasing strain of 4% (a), 6.4% (b), 6.5% (c), 6.6% (d), 6.8% (e), and 6.9% (f). Ti, and Al.

deformation. It can be found that the large lattice rotation occurs in the plastic deformation region, resulting in the bending interface [45]. Compared with the surrounding lattice regions, the large microrotation fields are observed in the interface region. The atoms in the γ phase exhibit a lower microrotation value than those at the interface, due to the interface bending brings up the strong strain than dislocation slip. Unlike the deformation gradient, the phase interface bears the load of the rotation around the y axis for the compatible plastic deformation. The pronounced rotation fields exist in these regions surrounding the interfaces. The above observation suggests the influence of the

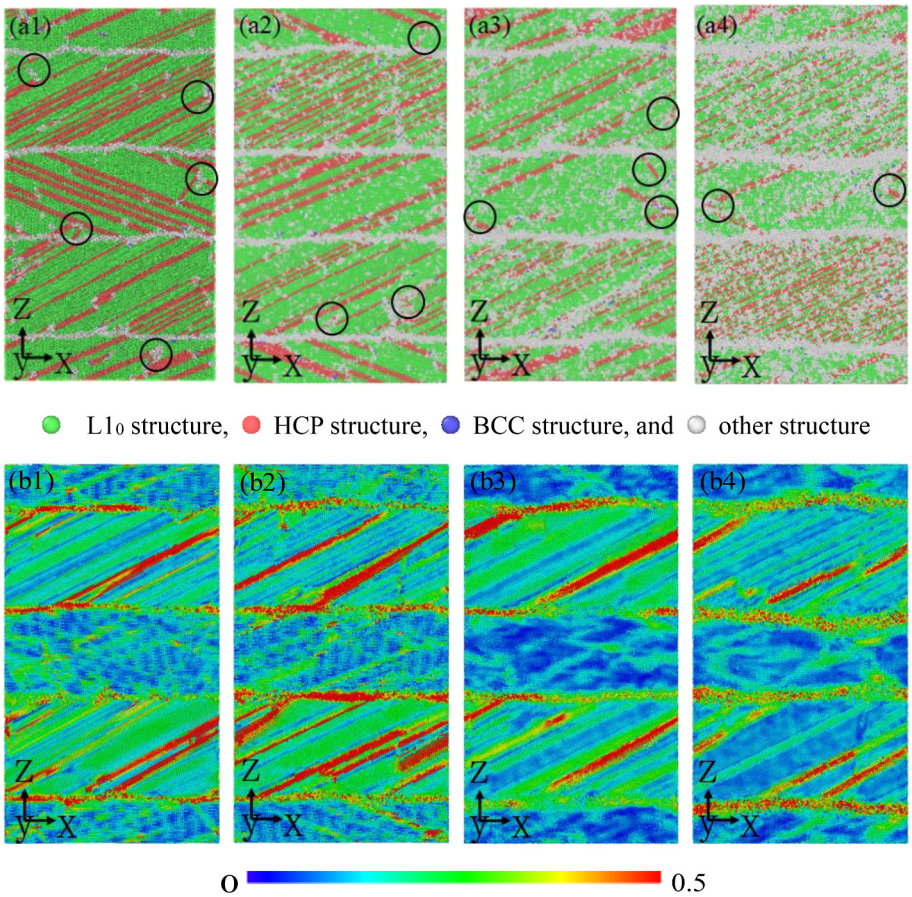

Fig. 7. The microstructure evolution, and the distribution of the corresponding strain for the temperatures of 300 K (a1, b1), 1100 K (a2, b2), 1300 K (a3, b3), and 1500 K (a4, b4) at the strain of 20%. The black circle indicates that the multi-slip systems are activated.

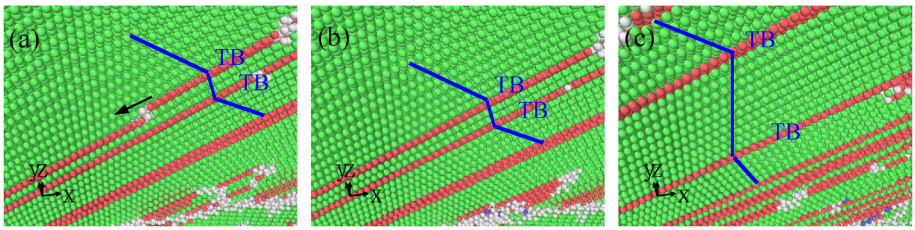

Fig. 8. The deformation twinning with the increasing strain. "TB" stands for twinning boundary. $L1_0$ structure, HCP structure, and other structure.

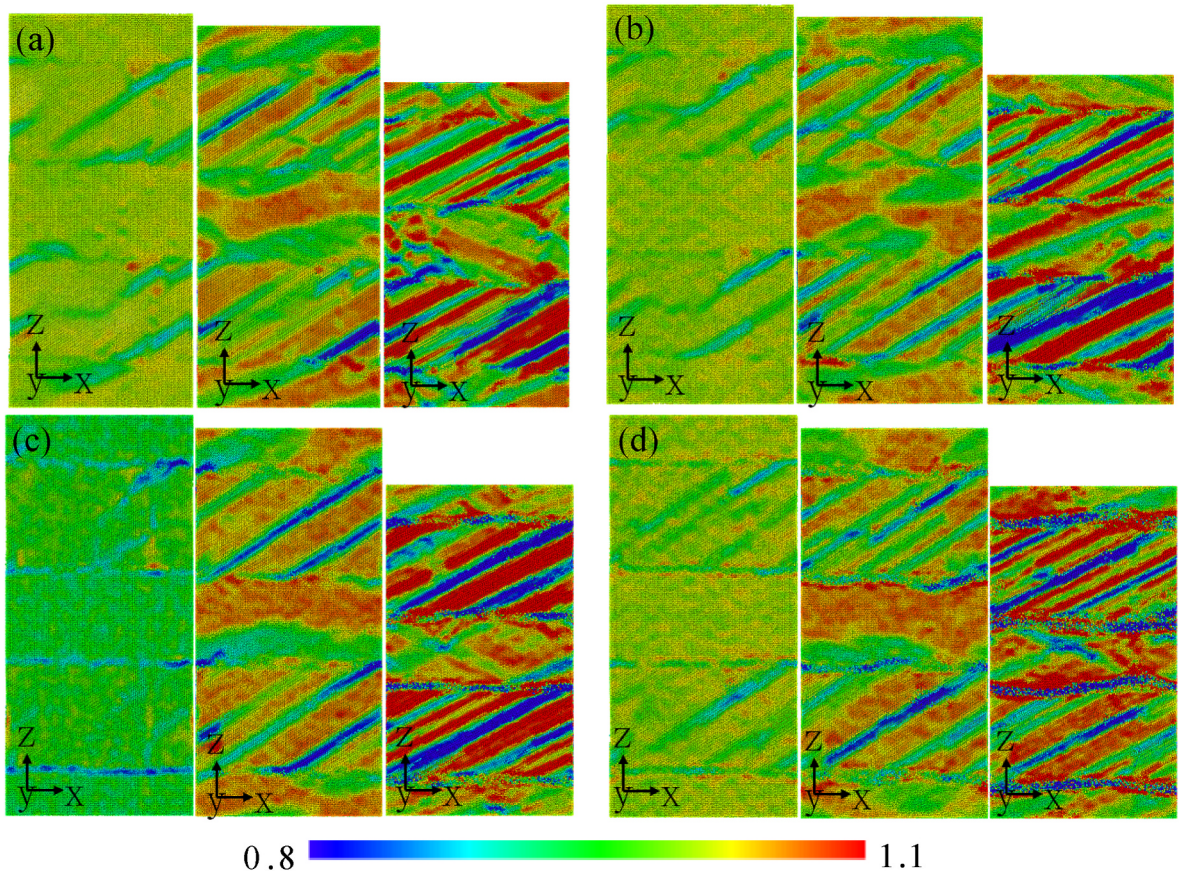

Fig. 9. The deformation gradient, zz, for the temperatures of 300 K (a), 1100 K (b), 1300 K (c), and 1500 K (d). For the given temperature, the strain is 3%, 6%, and 20%.

interfacial structure on the mechanical behavior of the nanolamellar composite in terms of the atomic-scale rotation and deformation gradient (Figs. 9 and 10). With the increasing strain, the high atomic-scale rotation around the y axis occurs along the interface. The higher temperature would increase the atomic-scale rotation around the y axis, inevitably improving the deformation capacity of materials (Fig. 10). Thus, the origin of the nanoscale plasticity event at a wide temperature range would be used for the reasonable regulation of the phase interface.

Fig. 11 shows the volume fraction for the large shear strain, rotation, and deformation gradient zz. As the temperature increases, both the shear strain and rotation monotonically increase, but the deformation gradient shows the opposite trend [45,46]. As the strain increases, the values of the shear strain, rotation and deformation gradient always rise. Especially, this interesting observation fades away due to the complex strain field induced by the microstructure at the large plastic deformation. Aside from the evolution of the shear strain and rotation, the deformation gradient may be the key factor to control the deformation of the nanolamellar TiAl/Ti_3Al composite. This trend is due to that a relatively small tangential translation of the left lattice with respect to the right lattice takes place during the large plastic deformation. The key continuum mechanical quantities of the shear strain, rotation, and deformation gradient can be quantified in the atomistic simulations. This result gives a meaningful and fundamental understanding about the interface phenomena integral to the nanolamellar composite deformation.

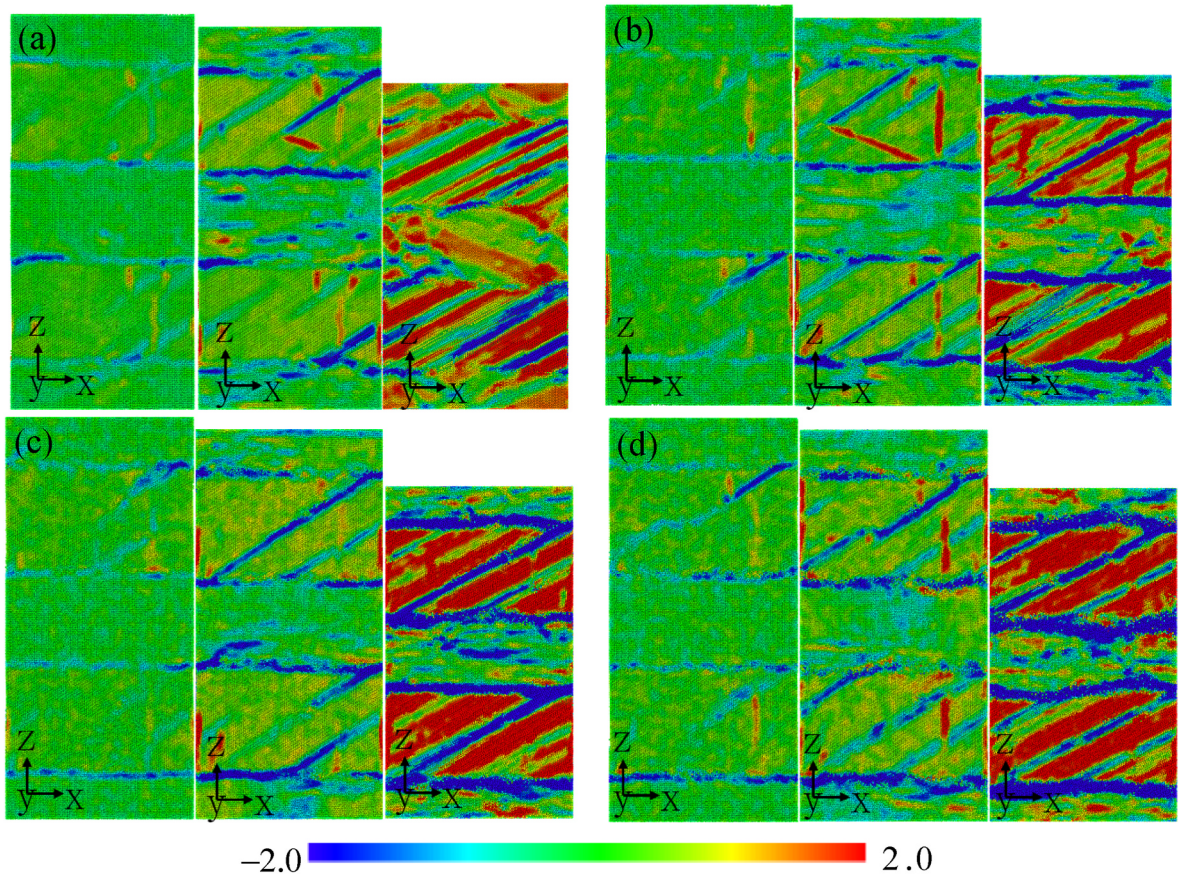

Fig. 10. The rotation around y axis with the increasing strain for the temperatures of 300 K (a), 1100 K (b), 1300 K (c), and 1500 K (d). For the given temperature, the strain is 3%, 6%, and 20%.

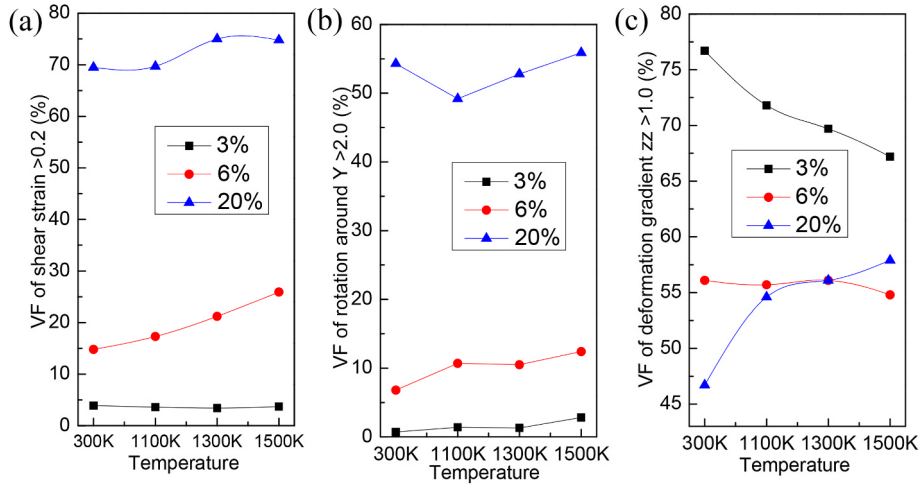

Fig. 11. The volume fraction in the shear strain >0.2 (a), rotation >2.0 (b), and deformation gradient zz > 1.0 (c) with the increasing temperature.

4. Conclusions

The present study highlights the role of temperature on deformation behavior in the nanolamellar TiAl/Ti_3Al composite using MD simulations. The results show that the phase interfaces are not only effective to promote the nucleation of phase transformation, but also control the dynamic grain growth. The softening stage is attributed to the deformation-induced $\alpha_2 \rightarrow \gamma$ phase transformation, and the strain hardening comes from the deformation twinning and activation of the multi-slip system. The atomic-scale deformation gradient field and the microrotation field dominate the nanoscale plasticity of the nanolamellar composite. These findings provide a better understanding of the role of the lamellar structure on the mechanical properties and deformation mechanism maps of the nanolamellar TiAl/Ti_3Al composite in a wide temperature range.

Author statement

Yang Chen: Investigation, Methodology, Validation, Visualization, Software, Writing - original draft, Writing - review & editing. **Jia Li:** Conceptualization, Investigation, Methodology, Validation, Visualization, Writing - original draft, Writing - review & editing, Project administration, Resources, Supervision. **Bin Liu:** Conceptualization, Investigation, Methodology, Validation, Visualization, Writing - original draft, Writing - review & editing, Project administration, Resources, Supervision. **Jian Wang:** Conceptualization, Investigation, Methodology, Validation, Visualization, Supervision. **Nan Liu:** Investigation, Data curation, Visualization, Supervision, Validation. **Siwei Ren:** Investigation, Methodology, Validation, Writing - original draft, Writing - review & editing. **Peter K. Liaw:** Investigation, Methodology, Funding acquisition, Supervision. **Qihong Fang:** Methodology, Software, Data curation, Visualization, Investigation, Writing – review & editing, Supervision.

Declaration of competing interest

The authors declare that they have no known competing financial interests or personal relationships that could have appeared to influence the work reported in this paper.

Data availability

Data will be made available on request.

Acknowledgements

The authors would like to deeply appreciate the supports from the National Natural Science Foundation of China (12072109, 11902113 and 12172123), and Natural Science Foundation of Hunan Province (2022JJ20001 and 2021JJ40032). PKL is supported by the National Science Foundation (DMR-1611180 and 1809640).

References

[1] G. Chen, Y.B. Peng, G. Zheng, Z.X. Qi, M.Z. Wang, H.C. Yu, C.L. Dong, C.T. Liu, Polysynthetic twinned TiAl single crystals for high-temperature applications, Nat. Mater. 15 (2016) 876–881.
[2] T. Klein, L. Usategui, B. Rashkova, M.L. No, J. San Juan, H. Clemens, S. Mayer, Mechanical behavior and related microstructural aspects of a nano-lamellar TiAl alloy at elevated temperatures, Acta Mater. 128 (2017) 440–450.
[3] H. Clemens, S. Mayer, Design, processing, microstructure, properties, and applications of advanced intermetallic TiAl alloys, Adv. Eng. Mater. 15 (2013) 191–215.
[4] W.G. Zhai, P. Wang, F.L. Ng, W. Zhou, S.M.L. Nai, J. Wei, Hybrid manufacturing of gamma-TiAl and Ti-6Al-4V bimetal component with enhanced strength using electron beam melting, Compos. Eng. B 207 (2021), 108587.
[5] Y.J. Hao, J.X. Liu, S.K. Li, J.C. Li, X.Z. Liu, X.Y. Feng, Effects of nano-twinning on the deformation and mechanical behaviours of TiAl alloys with distinct microstructure at elevated loading temperatures, Mater. Sci. Eng., A 5 (2017) 210–218.
[6] L. Chen, T.E.J. Edwards, F. Di Gioacchino, W.J. Clegg, F.P.E. Dunne, M.S. Pham, Crystal plasticity analysis of deformation anisotropy of lamellar TiAl alloy: 3D microstructure-based modelling and in-situ micro-compression, Int. J. Plast. 119 (2019) 344–360.
[7] P. Majumdar, S.B. Singh, M. Chakraborty, Elastic modulus of biomedical titanium alloys by nano-indentation and ultrasonic techniques A comparative study, Mater. Sci. Eng., A 489 (2008) 419–425.
[8] A.J. Palomares-Garcia, M.T. Perez-Prado, J.M. Molina-Aldareguia, Effect of lamellar orientation on the strength and operating deformation mechanisms of fully lamellar TiAl alloys determined by micropillar compression, Acta Mater. 123 (2017) 102–114.
[9] D. Wimler, J. Lindemann, T. Kremmer, H. Clemens, S. Mayer, Microstructure and mechanical properties of novel TiAl alloys tailored via phase and precipitate morphology, Intermetallics 138 (2021), 107316.
[10] M. Abdel-Hady, K. Hinoshita, M. Morinaga, General approach to phase stability and elastic properties of β-type Ti-alloys using electronic parameters, Scripta Mater. 55 (2006) 477–480.
[11] J. Ding, M.H. Zhang, Y.F. Liang, Y. Ren, C.L. Dong, J.P. Lin, Enhanced high-temperature tensile property by gradient twin structure of duplex high-Nb-containing TiAl alloy, Acta Mater. 161 (2018) 1–11.
[12] L. Cheng, Y. Chen, J.S. Li, E. Bouzy, Superplastic deformation mechanism of a gamma-TiAl alloy with coarse and bimodal grain structure, Mater. Lett. 194 (2017) 58–61.
[13] T. Ma, Q. Li, Y. Wang, X. Wang, D. Dong, D. Zhu, Microstructure and mechanical properties of micro-nano Ti2AlC-reinforced TiAl composites, Intermetallics 146 (2022), 107563.
[14] C. Cai, S. He, L.F. Li, Q. Teng, B. Song, C.Z. Yan, In-situ TiB/Ti-6Al-4V composites with a tailored architecture produced by hot isostatic pressing: microstructure evolution, enhanced tensile properties and strengthening mechanisms, Compos. Eng. B 164 (2019) 546–558.
[15] Z.H. Sun, J. Zhang, G.X. Xin, L. Xie, L.C. Yang, Q. Peng, Tensile mechanical properties of CoCrFeNiTiAl high entropy alloy via molecular dynamics simulations, Intermetallics 142 (2022), 107444.
[16] R. Nazemnezhad, M. Zare, S. Hosseini-Hashemi, Sandwich plate model of multilayer graphene sheets for considering interlayer shear effect in vibration analysis via molecular dynamics simulations, Appl. Math. Model. 47 (2017) 459–472.
[17] F. Zhao, J. Zhang, C.W. He, Y. Zhang, X.L. Gao, L. Xie, Molecular dynamics simulation on creep behavior of nanocrystalline TiAl alloy, Nanomaterials 10 (2020) 1693.
[18] M. Kanani, A. Hartmaier, R. Janisch, Stacking fault based analysis of shear mechanisms at interfaces in lamellar TiAl alloys, Acta Mater. 106 (2016) 208–218.
[19] J. Li, B. Xie, L. Li, B. Liu, Y. Liu, D. Shaysultanov, Q. Fang, N. Stepanov, P.K. Liaw, Performance-oriented multistage design for multi-principal element alloys with low cost yet high efficiency, Mater. Horiz. 9 (2022) 1518.
[20] T.D. Nguyen, S.J. Plimpton, Accelerating dissipative particle dynamics simulations for soft matter systems, Comput. Mater. Sci. 100 (2015) 173–180.
[21] S. Nosé, A unified formulation of the constant temperature molecular dynamics methods, J. Chem. Phys. 81 (1984) 511–519.
[22] W.G. Hoover, Canonical dynamics: equilibrium phase-space distributions, Phys. Rev. 31 (1985) 1695.
[23] A. Stukowski, Visualization and analysis of atomistic simulation data with OVITO the Open Visualization Tool, Model. Simulat. Mater. Sci. Eng. 18 (2010), 015012.
[24] D. Faken, H. Jónsson, Systematic analysis of local atomic structure combined with 3D computer graphics, Comput. Mater. Sci. 2 (1994) 279–286.
[25] R.R. Zope, Y. Mishin, Interatomic potentials for atomistic simulations of the Ti-Al system, Phys. Rev. B 68 (2003), 024102.
[26] S. Kim, S. Ryu, Effect of surface and internal defects on the mechanical properties of metallic glasses, Sci. Rep. 7 (2017) 1–10.
[27] Z.D. Sha, S.X. Qu, Z.S. Liu, T.J. Wang, H. Gao, Cyclic deformation in metallic glasses, Nano Lett. 15 (2015) 7010–7015.
[28] J. Li, Q.H. Fang, B. Liu, Y. Liu, Transformation induced softening and plasticity in high entropy alloys, Acta Mater. 147 (2018) 35–41.
[29] Q.H. Fang, Y. Chen, J. Li, C. Jiang, B. Liu, Y. Liu, P.K. Liaw, Probing the phase transformation and dislocation evolution in dual-phase high-entropy alloys, Int. J. Plast. 114 (2019) 161–173.
[30] J. Peng, L. Li, F. Li, B. Liu, S. Zherebtsov, Q.H. Fang, J. Li, N. Stepanov, Y. Liu, F. Liu, P.K. Liaw, The predicted rate-dependent deformation behaviour and multistage strain hardening in a model heterostructured body-centered cubic high entropy alloy, Int. J. Plast. 145 (2021), 103073.
[31] Y. Tian, J. Ding, X. Huang, H.R. Zheng, K. Song, S.Q. Lu, X.G. Zeng, Plastic deformation mechanisms of tension-compression asymmetry of nano-polycrystalline tial: twin boundary spacing and temperature effect, Comput. Mater. Sci. 171 (2020), 109218.
[32] R.C. Feng, M.M. Wang, H.Y. Li, Y.N. Qi, Q. Wang, Z.Y. Rui, Micromechanism of cold deformation of two-phase polycrystalline Ti-Al alloy with void, Mater. 12 (2019) 184.
[33] Q.X. Pei, M.H. Jhon, S.S. Quek, Z. Wu, A systematic study of interatomic potentials for mechanical behaviours of Ti-Al alloys, Comput. Mater. Sci. 188 (2021), 110239.
[34] F. Appel, H. Clemens, F.D. Fischer, Modeling concepts for intermetallic titanium aluminides, Prog. Mater. Sci. 81 (2016) 55–124.
[35] A. Denquin, S. Naka, Phase transformation mechanisms involved in two-phase TiAl-based alloys—I. Lambellar structure formation, Acta Mater. 44 (1996) 343–352.
[36] J.X. Zhang, H.Q. Ye, Deformation-induced alpha(2)<->gamma phase transformation in a Ti-48Al-2Cr alloy, J. Mater. Res. 15 (2000) 2145–2150.
[37] J.G. Wang, L.C. Zhang, G.L. Chen, H.Q. Ye, T.G. Nieh, Deformation-induced γ↔ α2 phase transformation in a hot-forged Ti–45Al–10Nb alloy, Mater. Sci. Eng., A 239 (1997) 287–292.
[38] J. Zhang, C. Teng, Z. Meng, H. Xu, L. Yang, D. Xu, R. Yang, Selection and mechanical evaluation of γ/γ boundary in γ-TiAl alloy, Intermetallics 126 (2020), 106946.
[39] A. Eghtesad, M. Knezevic, High-performance full-field crystal plasticity with dislocation-based hardening and slip system back-stress laws: application to modeling deformation of dual-phase steels, J. Mech. Phys. Solid. 134 (2020), 103750.
[40] J. Parkin, S. Birosca, Crystallographic orientation influence on slip system activation and deformation mechanisms in Waspaloy during in-situ mechanical loading, J. Alloys Compd. 865 (2021), 158548.
[41] X. Liu, L. Song, A. Stark, U. Lorenz, Z. He, J. Lin, F. Pyczak, T. Zhang, Deformation and phase transformation behaviors of a high Nb-containing TiAl alloy compressed at intermediate temperatures, J. Mater. Sci. Technol. 102 (2022) 89–96.
[42] A. Vinogradov, M. Heczko, V. Mazanova, M. Linderov, T. Kruml, Kinetics of cyclically-induced mechanical twinning in gamma-TiAl unveiled by a combination

of acoustic emission, neutron diffraction and electron microscopy, Acta Mater. 212 (2021), 116921.
[43] H.L. Hao, W.Z. Zhou, Y. Lu, D. Lau, Atomic arrangement in CuZr-based metallic glass composites under tensile deformation, Phys. Chem. Chem. Phys. 22 (2020) 313–324.
[44] R.I. Borja, Finite element simulation of strain localization with large deformation: capturing strong discontinuity using a Petrov-Galerkin multiscale formulation, Comput. Method Appl. 191 (2002) 2949–2978.
[45] J.A. Zimmerman, D.J. Bammann, H.J. Gao, Deformation gradients for continuum mechanical analysis of atomistic simulations, Int. J. Solid Struct. 46 (2009) 238–253.
[46] G.J. Tucker, J.A. Zimmerman, D.L. McDowell, Shear deformation kinematics of bicrystalline grain boundaries in atomistic simulations, Model. Simulat. Mater. Sci. Eng. 18 (2010), 015002.